Journal of Solid State Chemistry 183 (2010) 2166–2173

Contents lists available at ScienceDirect

Journal of Solid State Chemistry

journal homepage: www.elsevier.com/locate/jssc

Ethanol-assisted hydrothermal synthesis and electrochemical properties of coral-like β-$Co(OH)_2$ nanostructures

Shaochun Tang, Sascha Vongehr, Yang Wang, Lan Chen, Xiangkang Meng *

National Laboratory of Solid State Microstructures, Department of Materials Science and Engineering, Nanjing University, Nanjing 210093, PR China

ARTICLE INFO

Article history:
Received 10 April 2010
Received in revised form
16 July 2010
Accepted 18 July 2010
Available online 24 July 2010

Keywords:
Cobalt hydroxide
Nanostructures
Porosity
Hydrothermal
Electrochemical capacitance

ABSTRACT

Highly uniform, porous β-$Co(OH)_2$ nanostructures with an appearance reminding of certain spherical corals were synthesized via a facile, one-step hydrothermal route using ethanol–water mixtures as solvents. The rough surfaces of the nanostructures consist of numerous randomly distributed, interconnecting nanoflakes, resulting in a network-like structure with many cavities. The coral-like product has a high Brunauer–Emmet–Teller specific surface area of 163 m^2/g. The diameter of the coral-like β-$Co(OH)_2$ nanostructures is adjustable from 800 nm to 2 μm. The effects of the ethanol/water ratio, the Co^{2+} concentration, the hydrothermal temperature, and the reaction time on the formation of the coral-like structures were investigated. Cyclic voltammetry and galvanostatic charge–discharge tests show that the β-$Co(OH)_2$ possesses excellent capacitive properties. This is mainly attributed to the high porosity, which allows a deep penetration by electrolytes.

1. Introduction

Inorganic nanostructures (NSs) with well-defined sizes and complex morphologies have attracted considerable research efforts because of their size-, morphology-, and nanostructure-dependent properties [1]. In particular, hierarchical NSs of transition metal oxides and hydroxides are a hot topic due to their attractive structures, large surface-to-volume ratio, and accessible active interfaces. During the past decade, a wide variety of hierarchically structured metal oxides and hydroxides [2–4] have been investigated.

Among the transition metal hydroxides, cobalt hydroxides [$Co(OH)_2$] have versatile applications in catalysis, as electrochemical supercapacitors, in magnetic recording [5–7], and diverse other fields. For instance, $Co(OH)_2$ is an important electrode material [5,8] and can be used as an effective additive to improve the electrochemical properties of nickel hydroxide electrodes [9]. Additionally, $Co(OH)_2$ materials display catalytic and reversible electro chromic properties [10], are used in sensing applications, and show potential as organic magnetic materials [11]. Moreover, β-$Co(OH)_2$ has been investigated as a precursor for the preparation of cobalt oxide nanomaterials by a thermal conversion [12,13]. $Co(OH)_2$ is polymorphic and crystallizes into layered structures with two forms, α- and β-$Co(OH)_2$ [14,15]. The hydrotalcite-like α-phase is metastable and easily transforms into the stable brucite-like β-phase in strongly alkaline media. Owing to its stability and enhanced conductivity when transformed to β-CoOOH [3], β-$Co(OH)_2$ is often selected as an additive in alkaline secondary batteries.

The properties of $Co(OH)_2$ materials are closely associated with their microstructures. E.g. their electrochemical capacitance is significantly influenced by surface area and morphology because double layer and pseudo capacitances are both interfacial phenomena and pores allow a rapid transfer of electrolytes [16,17]. Therefore, much research is devoted to the control of their microstructure. Diverse synthetic methods, such as solution precipitation [18], precursor conversions [19], and electrodeposition [1], have been employed to prepare various NSs of cobalt hydroxides. $Co(OH)_2$ NSs with different morphologies including rod [20], needle [21], sheet [22], belt [13], and butterfly like shapes [20] have been obtained. There are already reports on three dimensional, hierarchical structures of $Co(OH)_2$, such as sisal-, dandelion-, and rose-like shapes [23], and flowerlike hollow core-shell structures [24]. However, a tighter control over the sizes and fine structure of the $Co(OH)_2$ is still desired, and the specific surface area is insufficient for many applications, for example if a high electrochemical capacitance [25,26] is aimed at.

Hydrothermal synthesis is widely employed to prepare various nanosized inorganic materials [27]. The hydrothermal technique provides a versatile route to control grain size, particle morphology, microstructure, and phase composition via adjusting parameters such as temperature, process duration, and pH value of the solution [28]. The reaction media also play a significant role [29]. Compared to the conventional hydrothermal/solvothermal

* Corresponding author. Fax: +86 25 8359 5535.
E-mail address: mengxk@nju.edu.cn (X. Meng).

0022-4596/$ - see front matter © 2010 Elsevier Inc. All rights reserved.
doi:10.1016/j.jssc.2010.07.030

process, in which usually only a single solvent is used, mixed solvents allow yet more control via adjusting the type and ratio of the solvents [30].

In this study, we report the synthesis of highly uniform, close to spherical, coral-like β-$Co(OH)_2$ NSs through a facile, ethanol-assisted hydrothermal process. This reliably reproducible method uses only $CoCl_2$, NaOH, and sodium tartrate as reactants without templates or further auxiliary reagents. The ratio of ethanol to water (r), the reaction temperature (T), the reaction time (t), and the $CoCl_2$ concentration (c) are important to ensure the formation of coral-like NSs. These β-$Co(OH)_2$ NSs exhibit a high specific capacitance due to their porous structure.

2. Experimental section

2.1. Chemicals and materials preparation

All chemicals were purchased from Nanjing Chemical Reagent Ltd., are of analytical grade purity, and used as received without further purification. Deionized water with a resistivity above 18.0 MΩ cm was used directly from a JL-RO100 Millipore-Q Plus water purifier. In a typical procedure, 60 mg cobaltous chloride ($CoCl_2 \cdot 6H_2O$) (2.5 mM), 0.86 g sodium tartrate ($Na_2C_4H_4O_6 \cdot 2H_2O$, 37.5 mM), and 1.00 g sodium hydroxide (NaOH, 0.25 M) were in this sequence one after another dissolved in ethanol–water mixed solvent (25 ml ethanol and 75 ml deionized water) at room temperature (r.t.). The ratio r will always denote the amount of ethanol divided by the amount of water *before* mixing, i.e. $r=1{:}3$ in the typical experiment. The resulting, sandy beige solution was transferred into a poly(tetrafluoroethylene) (Teflon)-lined autoclave of 88 ml to fill its volume half full. The autoclave was put into an oven, maintained at 120 °C for 12 h, and then allowed to cool to r.t. The black precipitate was collected and washed with deionized water and ethanol by several centrifuging/re-dispersion cycles. The product was dried in an oven for 8 h at 40 °C.

2.2. Physical measurements

The phase purity of the products was examined by X-ray powder diffraction (XRD) with a D/Max-RA X-ray diffractometer (using Cu$K\alpha=1.5418$ Å radiation). The size and morphology of the resulting products were observed by a Hitachi S-4800 field-emission scanning electron microscope (FE-SEM) at an acceleration voltage of 10.0 kV. Energy dispersed X-ray spectroscopy (EDS) was performed on the same FE-SEM. Transmission electron microscopy (TEM) images were taken on an FEI TECNAI F20 TEM operating at an acceleration voltage of 200 kV. X-ray photoelectron spectroscopy (XPS) was performed in a Thermo VG Scientific MultiLab ESCA2000 system with a CLAM4 hemispherical analyzer and at a base pressure below 3×10^{-10} mbar. Fourier transform infrared (FT-IR) spectra were recorded with a Varian 3100 FT-IR spectrometer using a KBr wafer. The specific surface area was estimated by the Brunauer–Emmet–Teller (BET) method based on nitrogen absorption–desorption (Micromeritics ASAP 2020). The desorption isotherm was used to determine the pore size distribution via the Barret–Joyner–Halender (BJH) method.

2.3. Electrochemical characterization

A working electrode of β-$Co(OH)_2$ was prepared by pressing a mixture containing 80 wt% β-$Co(OH)_2$ NSs product, 15 wt% acetylene black and 5 wt% polytetrafluoroethylene (PTFE) binder onto a nickel grid (1.2×10^7 Pa) that serves as a current collector (1 cm^2 surface). The typical mass load of electrode material is 5 mg. The electrochemical measurements were done in a three-electrode system with a platinum foil counter electrode and an Ag/AgCl reference. The used electrolyte was 2 M aqueous KOH solution. Cyclic voltammetry (CV) and galvanostatic charge–discharge (CD) tests employed an electrochemical work station (CHI-660, Chenhua, Shanghai). CV scans were recorded from 0 to 0.5 V (vs. Ag/AgCl) at different scan rates, and CD cycle tests were carried out in the range of 0–0.5 V at different currents. All measurements were carried out at r.t.

3. Results and discussion

Typical FE-SEM images of the as-prepared product ($t=12$ h) are presented in Fig. 1. The image of Fig. 1a indicates that the obtained particles are almost spherical and have a narrow size distribution with an average diameter of 1.6 μm. A magnified image (Fig. 1b) reveals that the particles display an appearance reminding of certain types of spherical corals. The surfaces show numerous randomly distributed, interconnecting flakes, resulting in a network-like structure with many cavities between the adjacent flakes (Fig. 1c). The flakes have a uniform thickness of ~30 nm. The flake-built NSs are similar to those of flowery architectures [7,26,31], nano-flake network [32] and loose-packed nano-flake materials [25]. Different from these reports, the nanoflakes in our NSs are interconnected instead of being stacked while at the same the whole structure is rather spherical. The EDS result (Fig. 1d) shows only the elements Co and O, and the inset reveals that the atomic percentage of Co (32.47%) is close to half that of oxygen (67.53%), as is expected from the $Co(OH)_2$ stoichiometry; both facts indicate a high purity of the products.

The chemical bonding states in the product were characterized by XPS measurements. The XPS spectra have been referenced to the C 1s peak at 284.2 eV. The binding energies of the Co 2p3/2 and 2p1/2 states are located at 781.4 and 797.5 eV, respectively, as illustrated in Fig. 2a (taken from sample shown in Fig. 1). The Co 2p main peaks have a satellite peak on the higher binding-energy side, which indicates a divalent state of Co ions in the product [33]. Compared with XPS established $Co(OH)_2$ binding energies of 781.3 and 797.3 eV in the literature [13], the Co 2p lines shifted by 0.1 and 0.2 eV to higher binding energies (Table 1). The binding energy of the O 1s state being at 531.0 eV (Fig. 2b) is consistent to the reported value and confirms the presence of O–H bonds [34].

The presence of the β-phase can be confirmed via FT-IR spectroscopy as depicted in Fig. 3. A narrow band is located at 3633 cm^{-1}, which corresponds to the νO–H stretching of the OH groups in the brucite-like structure. A broad band at about 3445 cm^{-1} is characteristic of the stretching vibration of interlayer water molecules and of hydroxyl groups hydrogen-bonded to H_2O [31]. The band at 1633 cm^{-1} corresponds to the bending mode of water molecules [35,36]. The peaks in the region of 490–540 cm^{-1} can be assigned to Co–O stretching vibrations and Co-OH bending vibrations in the brucite-like structure [37].

A typical TEM image of the product is shown in Fig. 4a. The particles consist of many flakes distributed around a denser core. A high-magnification TEM image (Fig. 4b) of an individual particle displays its loose, network-like structure made from sheets that reach far into the interior. The HRTEM image in Fig. 4c indicates that an individual flake has good crystallinity but is not single crystalline (various domains with different crystallographic orientations are marked with dashed circles). The distance between the lattice planes along a certain direction is measured to be 0.2369 nm, which is in accord with the (101) lattice spacing

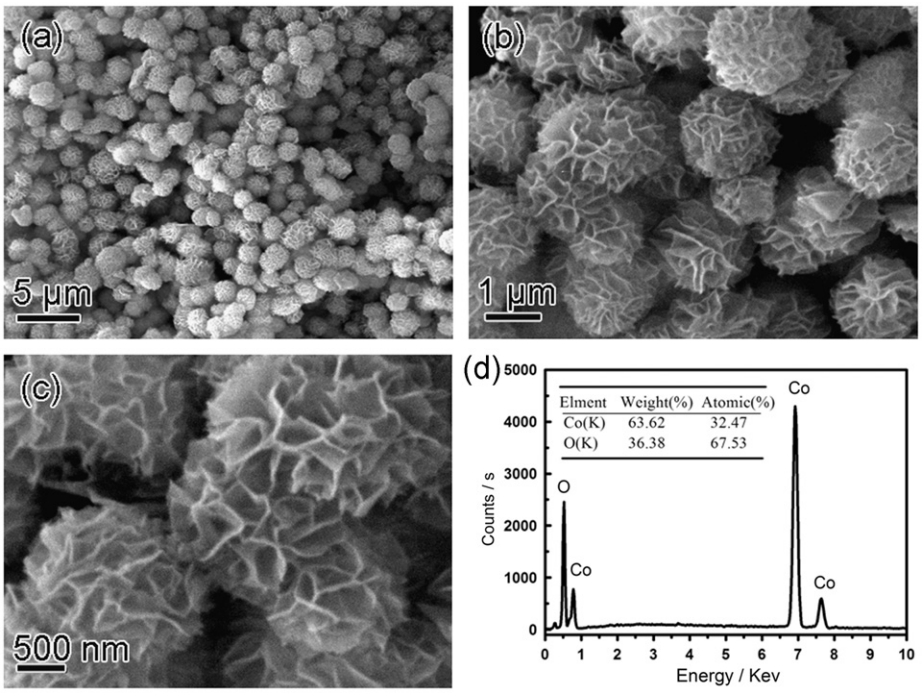

Fig. 1. Low- (a) and high-magnification (b,c) SEM images, and EDS spectrum (d) of the coral-like β-$Co(OH)_2$ NSs prepared under typical synthesis conditions (c=2.5 mM, r=1:3, T=120 °C, and t=12 h).

of β-$Co(OH)_2$ (d_{101}=0.2371 nm). Because of the random distribution of the flakes and the domains in individual flakes, an SAED pattern (Fig. 4d) recorded from one particle indicates its polycrystalline nature. The diffraction rings correspond to β-$Co(OH)_2$ (JCPDS 30-443).

Fig. 5 shows the morphology evolution of the products over reaction time t while c, r, and T were kept at 2.5 mM, 1:3, and 120 °C. A sample obtained after a short hydrothermal reaction of t=2 h contains dense spheres with diameters of about 150 nm (Fig. 5a). After 5 h (Fig. 5b), the resulting NSs have an average diameter of 0.8 μm and small surface flakes formed shells around the denser cores. After 8, 12, and 16 h of reaction time (Figs. 5c, 5d and 1c, respectively), the average diameter of the particles increased to 1.0, 1.6, and 2.0 μm, and the flakes grew gradually to form a rough, porous surface, resulting in the coral-like morphology. It can be seen from the insets of Figs. 5b and 5d that the number density of the flakes at the surface does not change with reaction time t, which implies that new flakes grow in between already present ones during the entire growth process. Thus, the size of the particles is controlled via selecting t, while the number density of the flakes and the related size of the gaps (cavities) between adjacent flakes stay uniform and can be addressed independently from the size by changing other parameters.

In this reaction system, ethanol is very important for the coral-like morphology. The strong influence is expected due to the fact that above about r=1:2, sodium tartrate does not dissolve in the mixed solvent. Without sodium tartrate, the reaction proceeds so fast that large aggregates of $Co(OH)_2$ precipitate immediately after the reaction regents are dissolved at r.t. Without ethanol (r=0), particles with large sizes and irregular shapes formed, as shown in Fig. 6a. A ratio of only 1:9 already leads to the formation of a few coral-like shapes, but the bulk still consists of large, irregular aggregates (not shown). At r=1:4, the large aggregates are absent, however, the porosity of the corals and the homogeneity of the sample suffers, and the number of flakes decreased (Fig. 6b). The value of r=1:3 leads already to difficulties in dissolving the tartrate at r.t., but it does produce the most homogeneous product, as is demonstrated by Fig. 1. In addition, we studied the effect of cobalt chloride concentration c while the other parameters remained typical (e.g. t=12 h). At a small concentration (c=1.5 mM), the sizes of particles are smaller and the yield lower. Flake-built structures were still obtained, but the product's surfaces do not show a dense layer of flake edges and enclosed cavities (Fig. 6c). A TEM image shown in the inset indicates that the particles seem to be constructed by many flakes radiating out from the rather loose center. Increasing the concentration, the product does not show the flake-built structure above about c=7.5 mM. When c is increased further, the corals disappear completely and larger dendrites appear instead (Fig. 6d). The products in Fig. 6a and d does not resemble those certain, spherical corals that look much like the product depicted in Fig. 1. We found that 2.5 mM Co^{2+} is most suitable to ensure the formation of homogeneously coral-like structures.

In the reaction temperature range of T=80–180 °C, the $Co(OH)_2$ particles are all flake-built coral-like structures. Changing temperature inside this range impacts the purity of the products. The XRD patterns of the products prepared at different temperatures are shown in Fig. 7. With otherwise equal conditions as in the synthesis of the sample shown in Fig. 1, if the temperature is only 80 °C, the products will not crystallize well. This can be inferred from the weak main peaks in the XRD pattern (curve a). When T was increased to 120 °C (curve b), the peaks' intensity becomes stronger. All the strong diffraction peaks can be indexed to a pure hexagonal phase of β-$Co(OH)_2$ according to JCPDS 30-443, as the 2θ scan's main peaks are at 18.92°, 32.98°, 37.68°, and 58.08°, corresponding to the (001), (100), (002), and (110) diffractions. The β-$Co(OH)_2$ is in the pure brucite-like phase with lattice parameters of a=3.18 Å, b=3.18 Å, and c=4.65 Å (JCPDS 74-1057). Only weak impurity peaks corresponding to Co_3O_4, which is the oxidation product of cobalt hydroxide, are observed. Increasing T to 160 °C (curve c) results in yet better crystallinity, but three relatively weak peaks corresponding to the (220), (400), and (440) diffractions of cubic Co_3O_4 (PDF 42-1467)

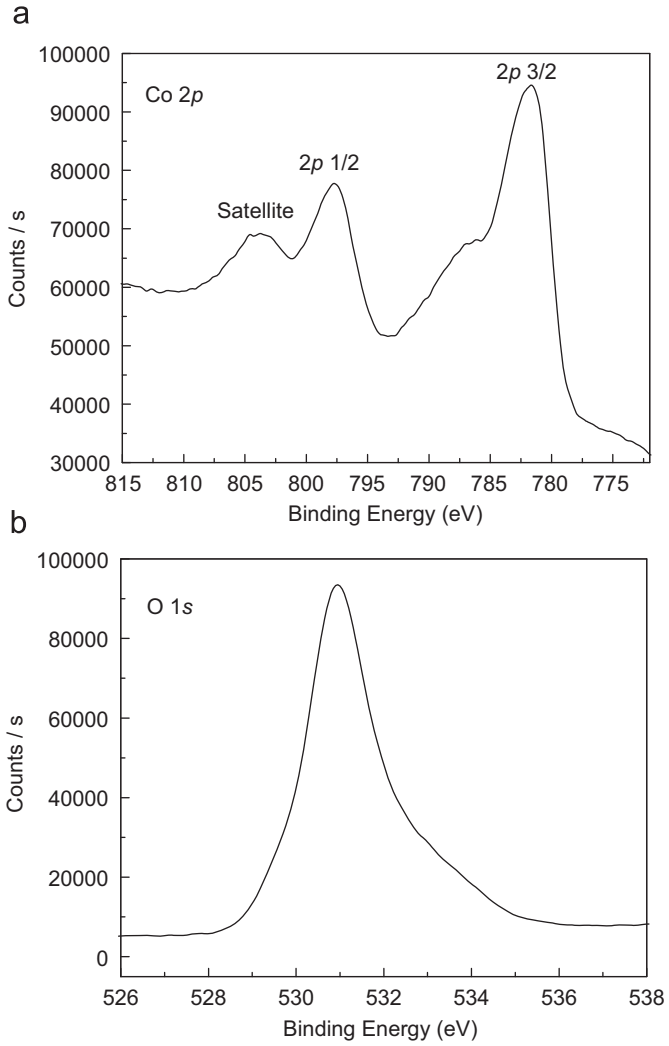

Fig. 2. XPS high-resolution spectra showing the Co 2*p* (a) and O 1*s* (b) related peaks.

Table 1
Binding energies (eV) for pure Co metal, oxides, and hydroxides.

Spectral region	Metal Co	CoO	$Co(OH)_2$	CoOOH	Co_3O_4	NSs product
Co 2*p* 3/2	778.2[a]	780.5[a]	781.3[a]	780.4[b]	779.9[b]	781.4
Co 2*p* 1/2	793.2[a]	796.3[a]	797.3[a]	802.4[b]	782.5[b]	797.5
O 1*s*	–	529.8[a]	529.6[c]	529.9[c]	530.0[b]	531.0

[a] From Ref. [31].
[b] From Ref. [13].
[c] From Ref. [32].

[38] also appear. When T was further increased to 180 °C, the crystallinity became much better, but also more Co_3O_4 formed (curve *d*).

To investigate the porosity of the $Co(OH)_2$ NSs, BET gas-sorption measurements were carried out. Fig. 8 shows the nitrogen adsorption-desorption isotherm of the coral-like β-$Co(OH)_2$ structures depicted in Fig. 1. The isotherm can be categorized as being of type IV with a distinct hysteresis loop [39,40], i.e. the pores are mostly in the interior rather than just on the surface. In other words, these pores should not be confused with the large (100–150 nm) cavities between the flakes' edges visible in the SEM images. The BET specific surface area is

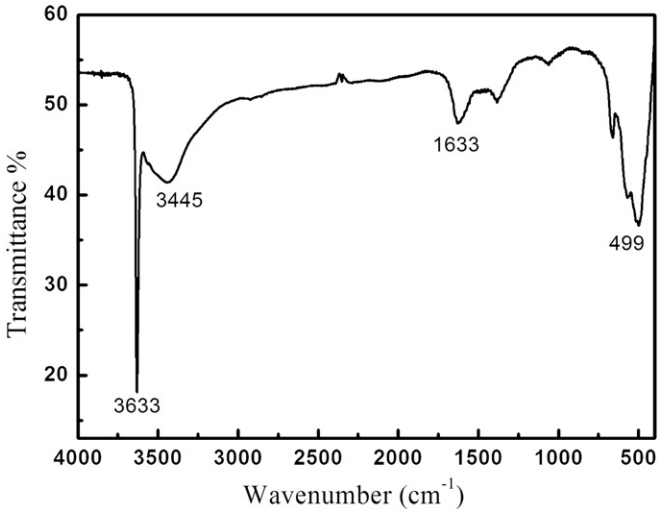

Fig. 3. FT-IR spectrum recorded from the coral-like NSs shown in Fig. 1.

163 m^2/g. The BJH adsorption average pore diameter of the β-$Co(OH)_2$ NSs is 14 nm, as can be calculated from the BJH pore diameter distribution presented in the inset.

Specific capacitance is correlated with the BET surface area and pore sizes [25]. The high porosity and specific surface area of the coral-like $Co(OH)_2$ particles promise super-capacitance. The capacitive behavior of the material was investigated by cyclic voltammetry (CV) and charge–discharge (CD) cycling. The specific capacitance (SC) based on CV and CD cycling can be calculated via [1]

$$SC_{CV} = Q/(m \times \text{potential range}) \quad (1)$$

$$SC_{CD} = I\Delta t/(m\Delta U) \quad (2)$$

Here, Q is anodic charge, I is the discharge current, Δt is the discharge time corresponding to the voltage difference (ΔU), and m is the electrode's active material mass. Fig. 9 shows typical CV curves of the $Co(OH)_2$ electrode prepared from the sample shown in Fig. 1, which were measured at scan rates of 5, 10, 20, and 50 mV/s. The shape of CV curves reveals that the capacitance characteristic is distinguished from that of the electric double-layer capacitance in which the shape is normally close to an ideal rectangular shape [39]. There are two pairs of redox peaks in the potential ranges of 0–0.25 and 0.25–0.4 V, indicating a pseudocapacitive behavior. This suggests that the capacitance is partially due to a Faradic reaction, which is an electrochemical adsorption/desorption or redox reaction at the interface between electrode material and electrolyte [39]. The voltammetric current gradually increases with the increase in the scan rate. They depend approximately linearly on the scan rate, as determined at various potentials.

Fig. 10a shows the CD characteristics of the coral-like $Co(OH)_2$ particle electrode in the 0–0.5 V potential range in 2 mol/L KOH at various specific current densities. The CD curves' symmetry implies a reversible reaction in the electrode material. There are two voltage regions that can be distinguished during the charging: Below about 0.3 V, the time dependence of the potential is linear, indicating the double-layer capacitance [41]. Above 0.3 V, the dependence is non-linear, indicating again the typical pseudo-capacitance behavior [41].

The variation of SC_{CD} with the specific current I_m is shown in Fig. 10b. The values of the coral-like $Co(OH)_2$ material at a specific current I_m of 0.5, 1.0, and 2.0 A/g are SC_{CD}=248, 225, and 197 F/g, respectively, as calculated from Eq. (2). That SC_{CD} decreases with increasing current is because the efficiency of redox reactions

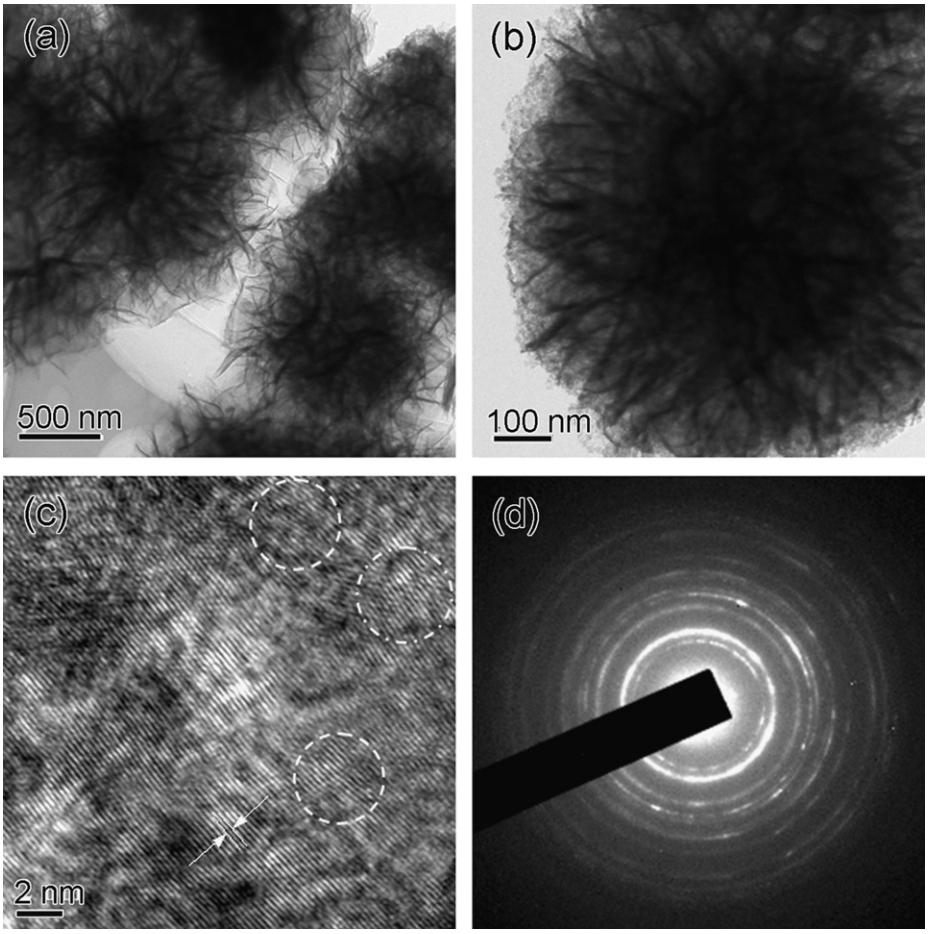

Fig. 4. TEM images (a, b), HRTEM image (c), and SAED pattern (d) of the coral-like β-$Co(OH)_2$ NSs (from the same sample shown in Fig. 1).

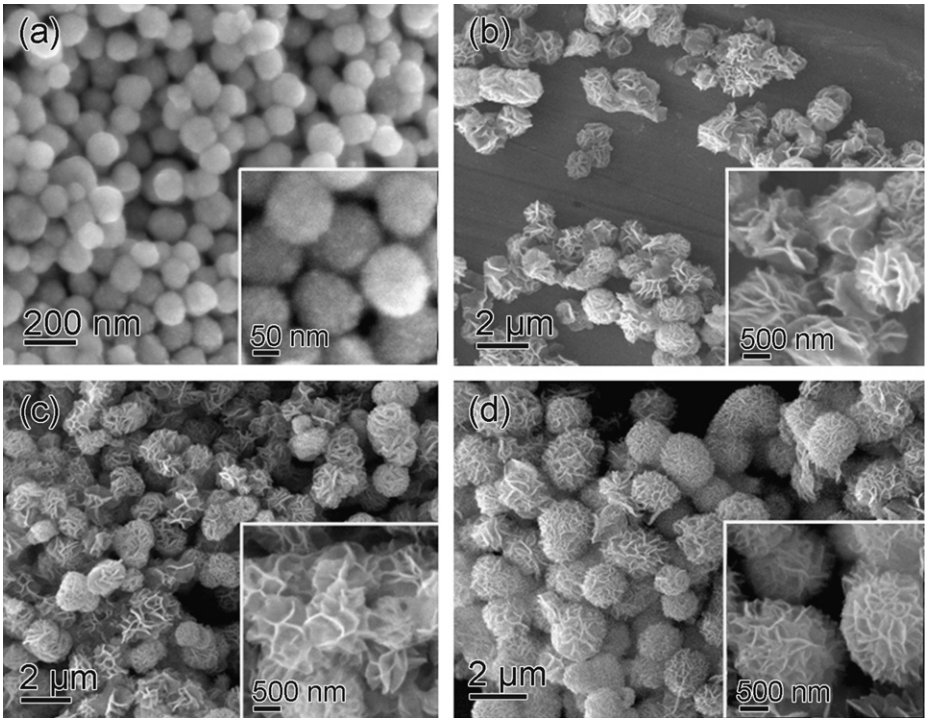

Fig. 5. FE-SEM images of the products prepared from different reaction times t of 2 h (a), 5 h (b), 8 h (c), and 16 h (d) while other conditions (c=2.5 mM, r=1:3, and T=120 °C) remained.

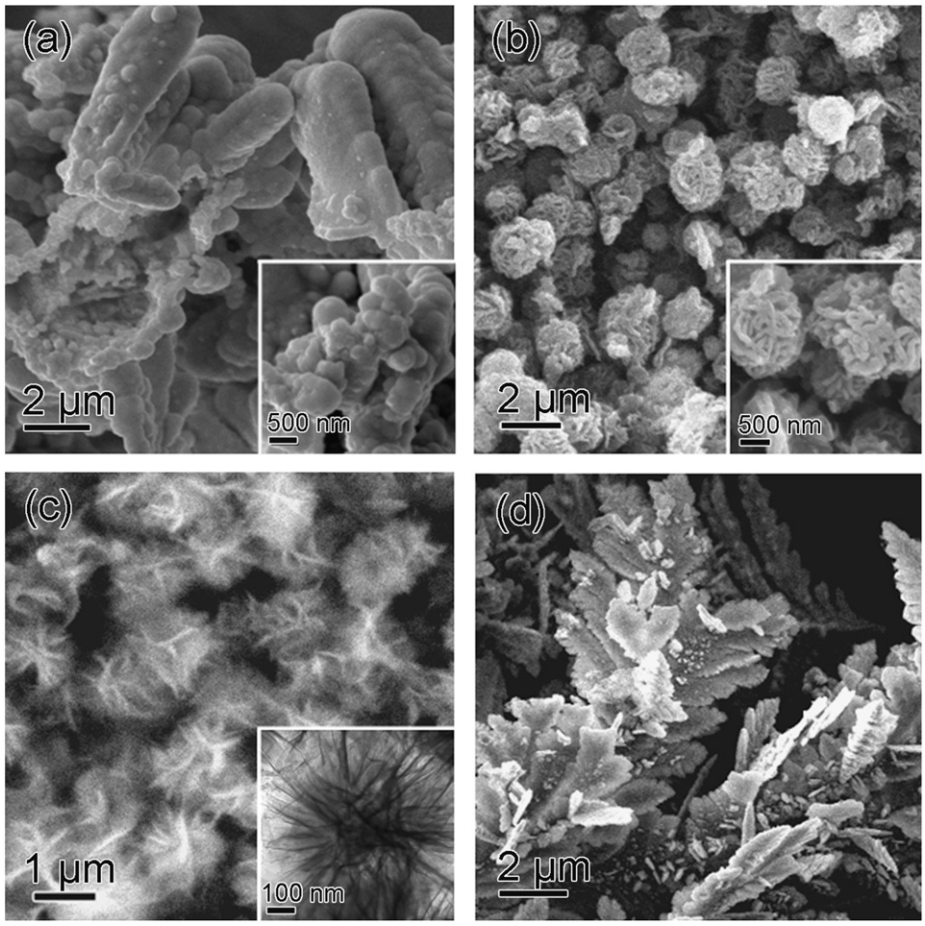

Fig. 6. SEM images of the product obtained without ethanol (a), r=1:4 (b), c=1.5 mM (c), and c=10 mM, while other conditions are the same as the typical synthesis. The insets of a, b are SEM images with higher magnifications; the inset of c is a high-magnification TEM image of an individual particle.

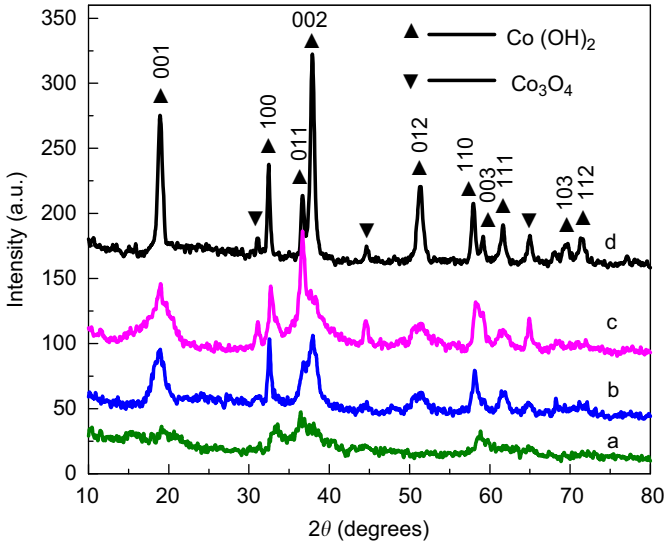

Fig. 7. XRD patterns of the NSs from hydrothermal synthesis at different reaction temperatures T of (a) 80, (b) 120, (c) 160, and (d) 180 °C while other conditions (c=2.5 mM, r=1:3, and t=12 h) remained.

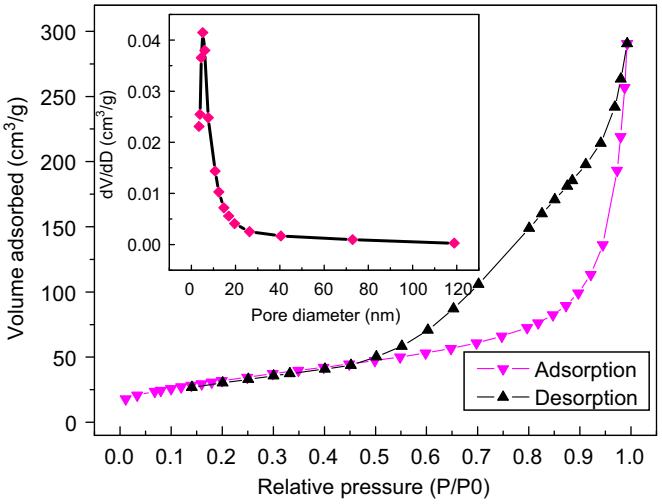

Fig. 8. Static adsorption–desorption isotherm hysteresis loop, and the pore diameter distribution (the inset) calculated using the BJH method.

decreases at high currents [1]. With I_m increasing to 1.0 and 2.0 A/g, the specific capacitance of coral-like β-$Co(OH)_2$ remains to be high at 90.73% and 79.5% of the capacitance at 0.5 A/g. This demonstrates the stability of the capacitance at high currents, which makes it attractive for many applications.

The reported specific capacity of flowery β-$Co(OH)_2$ materials at 5, 20, and 30 mA/g were 279, 174, 67 F/g, respectively [26]. Although the specific currents in our measurements are much higher, the specific capacity is still comparable to that of the flowery β-$Co(OH)_2$. The specific capacity of the coral-like β-$Co(OH)_2$ is much higher than that of $Co(OH)_2$ nanoparticles [26,42], $Co(OH)_2$-combined carbon-nanotube arrays [43], and

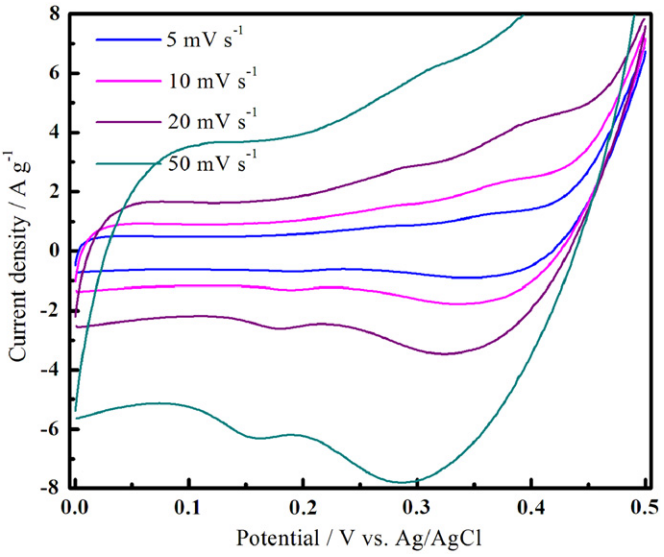

Fig. 9. Cyclic voltammetry (CV) curves at different scan rates within a potential window of 0–0.5 V vs. Ag/AgCl.

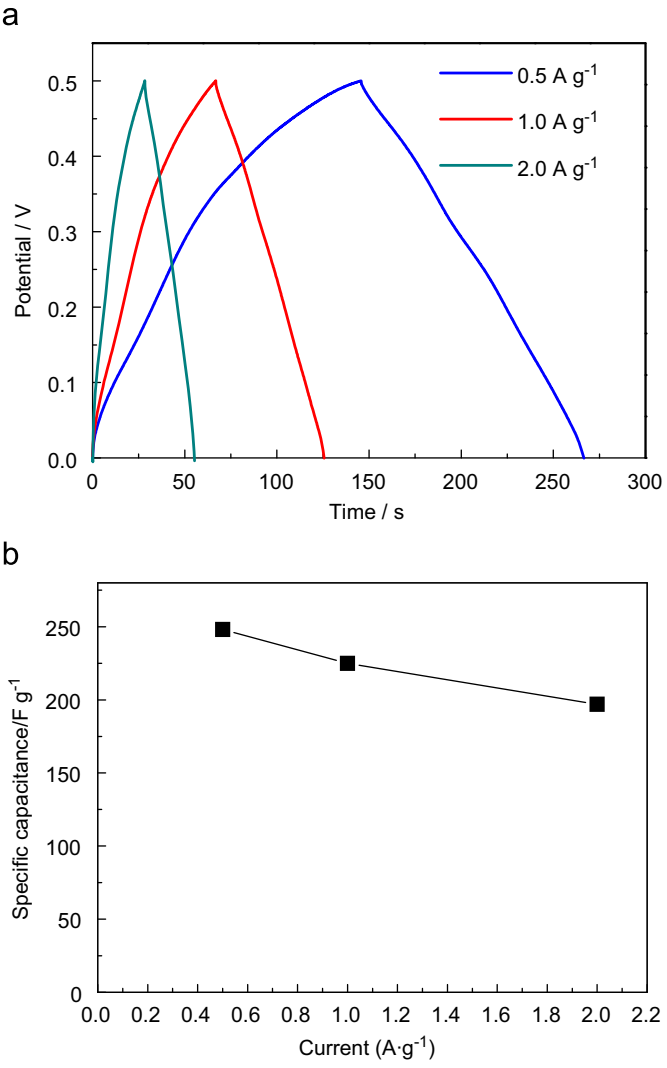

Fig. 10. Charge–discharge cycling curves in the potential range from 0 to 0.5 V in 2 mol/L KOH at different current densities (a), and the dependence of the SC_{CD} on current density (b) for the coral-like $Co(OH)_2$ NSs shown in Fig. 1.

CoOOH nanoflake films [17]. The obtained high specific capacitance is attributed to the high specific surface area of the porous nanostructure. High surface area allows interfacial phenomena (double layer and redox reactions) and pores provide channels for the electrolyte OH^- ions' diffusion [44].

4. Conclusions

Porous coral-like β-$Co(OH)_2$ NSs are synthesized via a template-free, one-step hydrothermal route using ethanol–water mixtures as solvents. The surfaces of the coral-like structures show numerous randomly distributed, interconnecting nanoflakes, resulting in a network-like structure with many cavities between the adjacent flakes. The diameter of the particles can be controlled by the reaction time t without altering the density of the flake structure. The optimal reaction parameters leading to homogeneously coral-like β-$Co(OH)_2$ particles include an ethanol/water ratio of r=1:3, a reaction temperature of T=120 °C, and a Co^{2+} concentration of c=2.5 mM. The β-$Co(OH)_2$ NSs have a large specific surface area and many pores, which facilitates the penetration by electrolytes and thus contributes to the excellent capacitive properties. The high specific capacity of 248 F/g is only little depressed by high currents. The capacitance can likely be improved upon in follow-up studies, which makes these materials interesting candidates for supercapacitors.

Acknowledgments

This work was jointly supported by a grant for the State Key Program for Basic Research of China (2010CB631004), the National Natural Science Foundation of China (50831004), the Innovation Fund of Jiangsu Province (BY2009148), and Doctoral Fund of Ministry of Education of China (20090091120034).

References

[1] X.W. Lou, D. Deng, J.Y. Lee, J. Feng, L.A. Archer, Adv. Mater. 20 (2008) 258–262.
[2] Y.Z. Shao, J. Sun, L. Gao, J. Phys. Chem. C 113 (2009) 6566–6572.
[3] Z.H. Jing, J.H. Zhan, Adv. Mater. 20 (2008) 4547–4551.
[4] E. Li, Z.X. Cheng, J.Q. Xu, Q.Y. Pan, W.J. Yu, Y.L. Chu, Cryst. Growth Des. 9 (2009) 2146–2151.
[5] V. Gupta, T. Kusahara, H. Toyama, S. Gupta, N. Miura, Electrochem. Commun. 9 (2007) 2315–2319.
[6] H.M. Chen, Y.Q. Zhao, M.Q. Yang, J.H. He, P.K. Chu, J. Zhang, S.H. Wu, Anal. Chim. Acta 659 (2010) 266–273.
[7] R. Qiao, X.L. Zhang, R. Qiu, J.C. Kim, Y.S. Kang, Chem. Eur. J. 15 (2009) 1886–1892.
[8] L. Cao, F. Xu, Y.Y. Liang, H.L. Li, Adv. Mater. 16 (2004) 1853–1856.
[9] W.Y. Li, S.Y. Zhang, J. Chen, J. Phys. Chem. B 109 (2005) 14025–14032.
[10] M. Dinamani, P.V. Kamath, J. Appl. Electrochem. 305 (2000) 1157–1161.
[11] A. Rujiwatra, C.J. Kepert, J.B. Claridge, M.J. Rosseinsky, H. Kumagai, M. Kurmoo, J. Am. Chem. Soc. 123 (2001) 10584–10594.
[12] Y.G. Li, B. Tan, Y.Y. Wu, J. Am. Chem. Soc. 128 (2006) 14258–14259.
[13] J.H. Yang, H. Hyodo, K. Kimura, T. Sasaki, Nanotechnology 21 (2010) 045605.
[14] D.L. Bish, A. Livingstore, Miner. Mag. 44 (1981) 339–343.
[15] P. Oliva, J. Leonardi, J.F. Laurent, C. Delmas, J.J. Braconnier, M. Figlarz, F. Fievet, J. Power Sources 8 (1982) 229–255.
[16] H. Zhou, D. Li, M. Hibino, I. Honma, Angew. Chem. Int. Ed. 14 (2005) 797–802.
[17] E. Hosono, S. Fujihara, I. Honma, M. Ichihara, H. Zhou, J. Power Sources 158 (2006) 779–783.
[18] Y.Y. Liang, L. Cao, L.B. Kong, H.L. Li, J. Power Sources 136 (2004) 197–200.
[19] F. Barde, M.R. Palacin, B. Beaudoin, A. Delahaye-Vidal, J.M. Tarascon, Chem. Mater. 16 (2004) 299–306.
[20] J.T. Sampanthar, H.C. Zeng, J. Am. Chem. Soc. 124 (2002) 6668–6675.
[21] L.Q. Zhang, A.K. Dutta, G. Jarero, P. Stroeve, Langmuir 16 (2000) 7095–7100.
[22] E. Hosono, S. Fujihara, I. Honma, J. Mater. Chem. 15 (2005) 1938–1945.
[23] B. Li, Y. Xie, C. Wu, Z. Li, J. Zhang, Mater. Chem. Phys. 99 (2006) 479–486.
[24] L.X. Yang, Y.J. Zhu, L. Li, L. Zhang, H. Tong, W.W. Wang, G.F. Cheng, J.F. Zhu, Eur. J. Inorg. Chem. 23 (2006) 4787–4792.
[25] L.B. Kong, J.W. Lang, M. Liu, Y.C. Luo, L. Kang, J. Power Sources 194 (2009) 1194–1201.

[26] X.M. Ni, H.G. Zheng, X.K. Xiao, X. Jin, G.X. Liao, J. Alloys Compds. 484 (2009) 467–471.
[27] X. Wang, J. Zhuang, Q. Peng, Y.D. Li, Nature 437 (2005) 121–124.
[28] S.C. Tang, Y.F. Tang, S. Vongehr, X.N. Zhao, X.K. Meng, Appl. Surf. Sci. 255 (2009) 6011–6016.
[29] H. Pang, F. Gao, Q.Y. Lu, Cryst. Eng. Commun. 12 (2010) 406–412.
[30] W.T. Yao, S.H. Yu, Adv. Funct. Mater. 18 (2008) 3357–3366.
[31] Z.A. Hu, Y.L. Xie, Y.X. Wang, L.J. Xie, G.R. Fu, X.Q. Jin, Z.Y. Zhang, Y.Y. Yang, H.Y. Wu, J. Phys. Chem. C 113 (2009) 12502–12508.
[32] L.B. Kong, J.J. Cai, L.L. Sun, J. Zhang, Y.C. Luo, L. Kang, Mater. Chem. Phys. 122 (2010) 368–373.
[33] T.J. Chuang, C.R. Bidle, D.W. Rice, Surf. Sci. 59 (1976) 413–429.
[34] J. Yang, H.W. Liu, W.N. Martens, R.L. Frost, J. Phys. Chem. C 114 (2010) 111–119.
[35] Z.P. Liu, R.Z. Ma, M. Osada, K. Takada, T. Sasaki, J. Am. Chem. Soc. 127 (2005) 13869–13874.
[36] Y.C. Zhu, H.L. Li, Y. Koltypin, A. Gedanken, J. Mater. Chem. 12 (2002) 729–733.
[37] Z.P. Xu, H.C. Zeng, Chem. Mater. 11 (1999) 67–74.
[38] Y. Lu, Y. Wang, Y.Q. Zou, Z. Jiao, B. Zhao, Y.Q. He, M.H. Wu, Electrochem. Commun. 12 (2010) 101–105.
[39] C.Z. Yuan, X.G. Zhanga, B. Gao, J. Li, Mater. Chem. Phys. 101 (2007) 148–152.
[40] J.F. Yao, H.T. Wang, J. Liu, K.Y. Chan, L.X. Zhang, N.P. Xu, Carbon 43 (2005) 1709–1715.
[41] H. Pang, Q.Y. Lu, Y.C. Lia, F. Gao, Chem. Commun. 48 (2009) 7542–7544.
[42] M.L. Zhang, Z.X. Liu, Chin. J. Inorg. Chem. 5 (2002) 513–517.
[43] H.J. Ahn, W.B. Kim, T.Y. Seong, Electrochem. Commun. 10 (2008) 1284–1287.
[44] W. Xing, F. Li, Z.F. Yan, G.Q. Lu, J. Power Sources 134 (2004) 324–330.